diagnostics

MDPI

Article

Two for One—Combined Morphologic and Quantitative Knee Joint MRI Using a Versatile Turbo Spin-Echo Platform

Teresa Lemainque [1,*], Nicola Pridöhl [1], Marc Huppertz [1], Manuel Post [1], Can Yüksel [1], Robert Siepmann [1], Karl Ludger Radke [2], Shuo Zhang [3,4], Masami Yoneyama [5], Andreas Prescher [6], Christiane Kuhl [1], Daniel Truhn [1] and Sven Nebelung [1]

[1] Department of Diagnostic and Interventional Radiology, Medical Faculty, RWTH Aachen University, 52074 Aachen, Germany; cyueksel@ukaachen.de (C.Y.); rsiepmann@ukaachen.de (R.S.); snebelung@ukaachen.de (S.N.)
[2] Department of Diagnostic and Interventional Radiology, University Hospital Düsseldorf, University Dusseldorf, 40225 Düsseldorf, Germany
[3] Philips GmbH Market DACH, 22335 Hamburg, Germany
[4] Philips Healthcare, 5684 PZ Best, The Netherlands
[5] Philips Japan, Tokyo 108-8507, Japan
[6] Institute of Molecular and Cellular Anatomy, Medical Faculty, RWTH Aachen University, 52074 Aachen, Germany
* Correspondence: tlemainque@ukaachen.de

Abstract: Quantitative MRI techniques such as T2 and T1ρ mapping are beneficial in evaluating knee joint pathologies; however, long acquisition times limit their clinical adoption. MIXTURE (Multi-Interleaved X-prepared Turbo Spin-Echo with IntUitive RElaxometry) provides a versatile turbo spin-echo (TSE) platform for simultaneous morphologic and quantitative joint imaging. Two MIXTURE sequences were designed along clinical requirements: "MIX1", combining proton density (PD)-weighted fat-saturated (FS) images and T2 mapping (acquisition time: 4:59 min), and "MIX2", combining T1-weighted images and T1ρ mapping (6:38 min). MIXTURE sequences and their reference 2D and 3D TSE counterparts were acquired from ten human cadaveric knee joints at 3.0 T. Contrast, contrast-to-noise ratios, and coefficients of variation were comparatively evaluated using parametric tests. Clinical radiologists (n = 3) assessed diagnostic quality as a function of sequence and anatomic structure using five-point Likert scales and ordinal regression, with a significance level of α = 0.01. MIX1 and MIX2 had at least equal diagnostic quality compared to reference sequences of the same image weighting. Contrast, contrast-to-noise ratios, and coefficients of variation were largely similar for the PD-weighted FS and T1-weighted images. In clinically feasible scan times, MIXTURE sequences yield morphologic, TSE-based images of diagnostic quality and quantitative parameter maps with additional insights on soft tissue composition and ultrastructure.

Keywords: magnetic resonance imaging; knee joint; quantitative imaging; cartilage

Citation: Lemainque, T.; Pridöhl, N.; Huppertz, M.; Post, M.; Yüksel, C.; Siepmann, R.; Radke, K.L.; Zhang, S.; Yoneyama, M.; Prescher, A.; et al. Two for One—Combined Morphologic and Quantitative Knee Joint MRI Using a Versatile Turbo Spin-Echo Platform. *Diagnostics* **2024**, *14*, 978. https://doi.org/10.3390/diagnostics14100978

Academic Editor: Aristeidis H. Zibis

Received: 14 March 2024
Revised: 25 April 2024
Accepted: 3 May 2024
Published: 8 May 2024

1. Introduction

Osteoarthritis (OA) is a chronic degenerative joint disease with a high prevalence and economic burden [1]. Cartilage degeneration is the structural hallmark of OA, while the surrounding tissues, i.e., menisci, bones, ligaments/tendons, and synovial tissue, are affected, too [2]. Magnetic resonance imaging (MRI) is the superordinate imaging modality to assess OA because it provides excellent soft tissue contrast [3].

The relaxation times T2 and T1ρ have been explored as surrogate markers of tissue composition, ultrastructure, and functionality of cartilage [2,4,5]. These parameters are sensitive to multiple constituents of cartilage at a time, but none is specific to a singular component [6]. For example, T2 was reported to correlate positively with water content and the orientation of collagen fibers, and negatively with the collagen and proteoglycan

content. Likewise, assessing these parameters can help detect early OA, i.e., when the damage may still be reversible [7,8]. T2 mapping, when added to the clinical routine protocol, increased the sensitivity of detecting early OA [9,10]. However, the clinical adoption of T2 and T1ρ mapping techniques is, among other factors, impeded by their long acquisition times, which may take 10 min or more to cover the whole joint [11].

Combined MRI sequences aim to solve this problem by providing (diagnostically useful) morphologic images alongside quantitative parameter maps in clinically feasible scan times. In knee joint imaging, the quantitative double-echo steady-state (qDESS) sequence provides T2 maps based on two gradient-echo images and takes 5 min to cover the whole joint [12]. The morphologic qDESS images enabled the comprehensive joint diagnosis with similar sensitivity, specificity, and accuracy compared to the conventional images [13]. However, the gradient-echo image contrast differs substantially from the turbo spin-echo (TSE) image contrast predominantly used clinically. Hence, Multi-Interleaved X-prepared Turbo Spin-Echo with IntUitive Relaxometry (MIXTURE) has been introduced as a sequencing platform to combine two or more TSE-based image contrasts with simultaneous T2 or T1ρ mapping. First preliminary studies [14–16] showed that whole-joint T2 and T1ρ mapping at isotropic resolution may be combined with morphologic image contrasts, e.g., proton density (PD)-weighted (-w) and T2-w fat-saturated (FS) images. Yoneyama et al. introduced the MIXTURE sequence platform and proposed two MIXTURE variants with isotropic resolution, i.e., a variant combining PD-weighted and T2-weighted FS imaging with T2 mapping and a variant combining PD-weighted and T1ρ-weighted FS imaging with T1rho mapping [14]. Sakai et al. undertook the sequence's preliminary clinical translation and investigated the first MIXTURE variant in thirteen patients with knee pain while providing example images of MIXTURE, 2D TSE, and 3D TSE reference sequences, respectively [15]. Saruya et al. combined the second variant with fluid attenuation and compared it to a gradient-echo-based T1rho mapping sequence in the knee, providing image examples and quantitative T1rho maps [16].

Nevertheless, beyond technical feasibility, certain aspects related to the sequence platform's clinical utilization, such as diagnostic quality and time demand, remain to be elucidated. Consequently, we aimed to (i) develop and refine MIXTURE sequence variants to match our institution's standard knee protocol and (ii) evaluate these variants versus the corresponding 2D and 3D TSE reference sequences in basic and translational research contexts, including a reader study to assess diagnostic quality. We hypothesized that MIXTURE sequences provide (i) morphologic images with characteristic TSE-based contrasts and sufficient diagnostic quality and (ii) quantitative maps simultaneously with only moderately increased time demand.

2. Materials and Methods

2.1. Study Design and Sample Size Estimation

The local Institutional Review Board approved this prospective in situ imaging study on human cadaveric knee joint specimens (Ethical Committee, RWTH Aachen University, EK180/16), which was conducted in accordance with relevant guidelines and regulations. The body donors had given written informed consent prior to the study. Assuming an inter-sequence difference in diagnostic quality scores of 0.5, an inter-specimen standard deviation (SD) of 0.4, a power of 0.8, and a significance level of 0.01, the minimum sample size was determined as eight. Ten fresh-frozen and non-fixated specimens were provided through the local anatomy department. We defined moderate-to-severe cartilage degeneration, such as substantial tissue loss or focal lesions, as an exclusion criterion. Before MR image acquisition, the specimens were left to thaw at room temperature for 24 h.

2.2. MR Image Acquisition

The MIXTURE technique uses interleaved 3D TSE sequence blocks of two or more image weightings, resulting in two (or more) differently weighted stacks of 3D TSE images. Consequently, quantitative maps are reconstructed for each slice. Image weightings are freely adjustable by selecting a preparation module, i.e., none, T2 preparation, or T1ρ preparation,

and prepulse, i.e., none, inversion recovery (IR), or spectral attenuated inversion recovery (SPAIR) (Figure 1a). Inspired by our clinical protocol of 2D TSE sequences, i.e., PD-w FS and T1-w sequences, two MIXTURE sequences were set up: (i) MIXTURE PD-w FS with T2 mapping (termed "MIX1") and (ii) MIXTURE T1-w with T1ρ mapping (termed "MIX2").

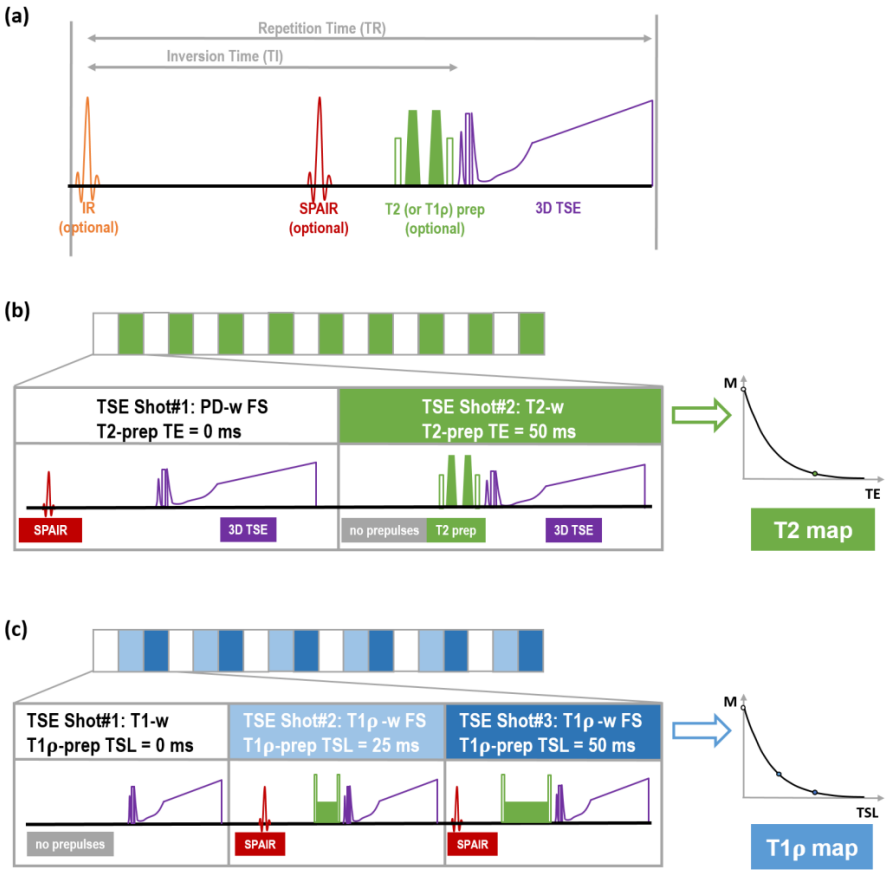

Figure 1. MIXTURE sequence platform. The MIXTURE sequence platform allows 3D TSE imaging with flexible preparation. (**a**) The basic building block of the sequence consists of optional T2 (or T1ρ) preparation (prep) modules and optional inversion recovery and/or SPAIR fat saturation prepulse to realize variable contrast weightings. (**b**) The MIXTURE PD-weighted (-w) fat-saturated (FS) sequence with T2 mapping interleaves TSE shots without (white blocks) and with T2 preparation (green blocks). In the PD-w FS block, an SPAIR prepulse is activated. Based on the resulting PD-w FS and T2-w images, T2 maps are calculated. (**c**) The MIXTURE T1-w sequence with T1ρ mapping interleaves TSE shots without (white blocks) and with T1ρ preparation modules of different spin lock times (TSL) (light blue and dark blue blocks). In the T1ρ-w FS blocks, an SPAIR prepulse is activated. Based on the resulting T1-w and T1ρ-w FS images, a T1ρ map is calculated. Abbreviations: MIXTURE—Multi-Interleaved X-prepared Turbo Spin-Echo with IntUitive Relaxometry, SPAIR—Spectral Attenuated Inversion Recovery.

For MIX1, as shown in Figure 1b, two TSE blocks were interleaved using a repetition time (TR) of 1200 ms. The first TSE block was configured without any relaxation preparation module, i.e., setting the echo time (TE) of the T2 preparation module to 0 ms, but with an SPAIR prepulse, resulting in PD-w FS images. The second TSE block was configured without an SPAIR prepulse but with a T2 preparation module using a TE of 50 ms, resulting in T2-w images. Based on the two images, T2 maps were reconstructed on the scanner workstation by fitting a mono-exponential signal decay function to the two TE values in a voxel-wise manner.

For MIX2, as shown in Figure 1c, three TSE blocks were interleaved using a TR of 600 ms. The first TSE block was configured without an SPAIR prepulse and by setting the

spin lock time (TSL) of the T1ρ preparation module to 0 ms, resulting in T1-w images. The second and third blocks were configured with an SPAIR prepulse and T1ρ preparation modules of TSL = 25 ms and TSL = 50 ms, respectively, at an offset frequency of 500 Hz, resulting in T1ρ-w FS images. Based on the three images, T1ρ maps were reconstructed as detailed above.

Our standard protocol's PD-w FS and T1-w 2D TSE sequences and the corresponding 3D TSE sequences were acquired using the same basic image acquisition parameters, i.e., slice orientation, slice thickness, number of slices, acquisition matrix, and reconstruction matrix, to permit voxel-to-voxel comparisons. Consequently, despite their 3D nature, the MIXTURE and the 3D TSE sequences were acquired non-isotropically with lower through-plane resolution (i.e., thicker slices) and higher in-plane resolution than previously published variants [14–16].

Table 1 summarizes the sequence parameters.

Table 1. MRI sequence parameters. MIXTURE sequences combine morphologic imaging with quantitative parameter mapping. The sequences were acquired as PD-w FS images with quantitative T2 maps ("MIX 1") and as T1-w images with T1ρ maps ("MIX 2"). Corresponding 2D TSE and 3D TSE reference sequences of the same image weightings were acquired, too.

Sequence Parameter	MIX 1	2D TSE PD-w FS	3D TSE PD-w FS	MIX 2	2D TSE T1-w	3D TSE T1-w
Sequence type	3D TSE	2D TSE	3D TSE	3D TSE	2D TSE	3D TSE
Orientation	Sagittal					
TR [ms]	1200	3000	1100	600	582	400
TE [ms]	N/A	40	N/A	N/A	15	N/A
TE_{eff} [ms]	125	N/A	125	22	N/A	36
TE_{equiv} [ms]	46	N/A	46	13	N/A	21
Echo train length [n]	35	11	35	12	5	8
Refocusing pattern	"MSK PD FS"	"no"	"MSK PD FS"	"Spine View T1"	"constant" (110°)	"MSK T1"
Compressed SENSE factor	4.5	2.5	3.5	6	2	6
NSA [*n*]	1	2	1	1	2	2
Fat saturation [1st block–2nd block]	SPAIR–none	SPIR	SPAIR	None–SPAIR	none	none
T2 preparation module TE [ms]	0 and 50	N/A	N/A	N/A	N/A	N/A
SL preparation module TSL [ms]	N/A	N/A	N/A	0 and 25 and 50	N/A	N/A
SL frequency [Hz]	N/A	N/A	N/A	500	N/A	N/A
Scan time [min:s]	4:59	4:06	2:57	6:38	4:23	4:22
FOV [mm^2]	140 × 140					
Acquisition matrix [px]	304 × 304					
Reconstruction matrix [px]	512 × 512					
Fat shift direction	Anteroposterior					
Phase oversampling [%]	12 + 12	30 + 30	12 + 12	12 + 12	33 + 33	12 + 12
Slices [n]	43					
Slice thickness [mm]	3					
Slice oversampling [%]	12	N/A	12	100	N/A	12

Abbreviations: MIXTURE—Multi-Interleaved X-prepared Turbo Spin-Echo with IntUitive Relaxometry, PD—proton density, FS—fat-saturated, TSE—turbo spin-echo, TR—repetition time, TE—echo time, SENSE—sensitivity encoding, NSA—number of signal averages, SPAIR—spectral attenuated inversion recovery, SPIR—spectral presaturation with inversion recovery, N/A—not applicable, SL—spin lock, TSL—spin lock time, FOV—field of view. For 3D TSE sequences, TEeff and TEequiv denote the effective and equivalent TE as mediated by the choice of the refocusing pattern. For the 2D TSE sequence that uses a constant refocusing flip angle, TE can be described by a single value.

2.3. Comparative Image Analysis

2.3.1. Image Contrast and Signal Quality

Region of interest (ROI)-based comparisons between sequences were similarly performed on a per-joint and per-sequence basis. ROI placement was standardized for all sequences: NP, a pre-graduate medical student with two years of experience in MRI, placed the ROIs, which TL, a medical imaging scientist with eight years of experience in MRI, reviewed subsequently.

To evaluate image contrast and contrast-to-noise ratio (CNR), two circular ROIs with a standard area (2.11 mm^2) were positioned in predefined anatomic structures. In the PD-w FS images, ROIs were placed within the femoral cartilage (central weight-bearing region of the lateral compartment) and the synovial fluid of the patellofemoral and femorotibial joint compartment. In the T1-w images, ROIs were placed within the femoral cartilage and the central infrapatellar fat pad.

Weber contrast [17] was used as a surrogate of image contrast and calculated based on the signal intensity of cartilage versus synovial fluid or fatty tissue:

$$C_w^{\text{PDw FS}} = \frac{SI_{cart} - SI_{syn}}{SI_{syn}} \quad (1)$$

and

$$C_w^{T_1w} = \frac{SI_{cart} - SI_{fat}}{SI_{fat}} \quad (2)$$

where SI_{cart}, SI_{syn}, and SI_{fat} are the mean signal intensities of the cartilage, synovial fluid, and fat pad ROIs.

CNR was used to quantify how distinguishable two structures are from the noise floor. Higher CNR values indicate that the two structures are more clearly distinguishable. CNR was calculated as

$$CNR^{\text{PDw FS}} = \frac{|SI_{cart} - SI_{syn}|}{\sqrt{\sigma_{cart}^2 + \sigma_{syn}^2}} \quad (3)$$

and

$$CNR^{T_1w} = \frac{|SI_{cart} - SI_{fat}|}{\sqrt{\sigma_{cart}^2 + \sigma_{fat}^2}}, \quad (4)$$

respectively, where σ_{cart}, σ_{syn}, and σ_{fat} are the standard deviations of the cartilage, synovial fluid, and fat pad ROIs.

As a surrogate for the signal-to-noise ratio, the coefficient of variation (CV) was quantified [18]. A circular ROI with an area of 3.76 mm^2 was positioned in a homogeneous area of the synovial fluid (PD-w FS images) or infrapatellar fat pad (T1-w images). CV was calculated as

$$CV^{\text{PD-w FS}} = \frac{\sigma_{syn}}{SI_{syn}} \quad (5)$$

and

$$V^{\text{T1-w}} = \frac{\sigma_{fat}}{SI_{fat}} \quad (6)$$

respectively. Higher CV values indicate stronger noise. No CV was calculated for cartilage because of its distinct layer structure, which is likely to make tissue inhomogeneity dominate over the statistical signal fluctuations.

2.3.2. Reader Study

Three clinical radiologists (MH, MP, CY) with 3, 4, and 4 years of clinical experience rated the images on in-house radiology workstations. The images were presented head-to-head using the in-house picture archiving and communication (PACS) system (iSite, Philips, Best, The Netherlands). MIX 1 (i.e., the MIXTURE PD-w FS image, MIXTURE T2-w image [TE = 50 ms], and MIXTURE T2 maps) were presented alongside the corresponding

2D and 3D TSE PD-w FS images. Analogously, MIX 2 (i.e., the MIXTURE T1-w image, MIXTURE T1ρ-w FS image [TSL = 50 ms], and MIXTURE T1ρ maps) were presented alongside the corresponding 2D and 3D TSE T1-w images. The parameter maps had been prepared as video files in Python (version 3.9.9), using the "jet" color map and fixed ranges (0 ms–100 ms [T2 map], 0 ms–70 ms [T1ρ map]), to allow for scrolling on a separate screen.

The radiologists semiquantitively rated the images on a per-sequence and per-joint basis. The diagnostic evaluability of different knee joint structures was quantified using an ordinal 5-point Likert scale, where score 1 indicated "very low evaluability", score 2 "low evaluability", score 3 "intermediate evaluability", score 4 "high evaluability", and score 5 "very high evaluability". These structures were selected as suggested by Chaudhari et al. [13]. The radiologists assigned lower scores to structures they would usually not primarily evaluate on a given sequence or orientation. In addition, image quality, contrast resolution, and anatomic delineation were synoptically assessed as a global diagnostic quality score for each sequence on a per-joint basis, using a similar ordinal 5-point Likert scale that extended from "very poor" (score 1) to "very good" (score 5). Also, the radiologists were instructed to note the presence of artifacts (i.e., suspicious features or distortions) in the morphologic 3D TSE or MIXTURE images compared to the 2D TSE images. Consequently, blinding to sequence type was not feasible. Moreover, the radiologists indicated whether the availability of the quantitative parameter map had increased their diagnostic confidence.

2.4. Quantitative Mapping

The femoral and tibial cartilage plates were segmented on the central slice of the lateral compartment based on the sagittal MIXTURE PD-w FS images. The segmentations were performed by NP using the Program ITK-Snap (v3.6, [19]), and reviewed by SN, a musculoskeletal radiologist with more than ten years of experience in MSK radiology. Mean T2 and T1rho values within the segmented areas and their standard deviations were calculated.

2.5. Statistical Analysis

NP, TL, KLR, and SN performed the statistical analyses. Separate inter-sequence comparisons between MIXTURE, 2D TSE, and 3D TSE were completed for the PD-w FS and the T1-w images. Diagnostic evaluability scores and the global diagnostic quality scores were analyzed in R (v4.0.3, R Foundation for Statistical Computing, Vienna, Austria) using mixed-effects ordinal regression, i.e., the Cumulative Link Mixed Model (CLMM) from the "ordinal" package. The sequence was the independent variable, while structure, reader, and joint specimen were set as random variables. The model was fitted using the Laplace approximation. Another CLMM was fitted to compare the global diagnostic quality scores between sequences. For both models, estimated marginal means (EMM) were calculated and compared post hoc using Tukey's multiplicity-adjusted post hoc test. EMMs represent the model-predicted response for each level of a variable, while averaging over other variables [20]. In the context of CLMMs, EMM values are defined on a latent scale [21], i.e., they do not directly relate to the ordinal response variable. Still, higher EMM values indicate higher values of the respective variable. Weber contrast, CNR, and CV were compared using Graph Pad Prism software (v9.5.1, San Diego, CA, USA) and repeated measures analysis of variance (ANOVA) followed by the Tukey–Kramer post hoc test. Multiplicity-adjusted p-values were computed to account for multiple comparisons. A family wise alpha error threshold of $p \leq 0.01$ was chosen to limit the number of statistically significant, yet clinically (most likely) non-significant findings.

3. Results

3.1. Study Cohort

All ten knee joint specimens (age 81.1 ± 10.4 years [mean ± standard deviation]; range 68–96 years; 9/1 male/female; 6/4 right/left joints) could be imaged per the study protocol.

3.2. Two-Dimensional TSE PD-Weighted FS Images Showed Most Pronounced Cartilage–Synovia Contrast

Across the acquired sequences, cartilage demonstrated an intermediate signal intensity and a layered zonal structure (Figure 2 and Figure S1). However, the ROI-based analysis yielded a significantly more pronounced contrast as evidenced by significantly more negative Weber contrast values between cartilage and synovia for the 2D TSE images ($p < 0.001$ [Figure 3a]). In visual terms, the negative Weber contrast values translate into a darker presentation of the cartilage tissue than the bright synovial fluid. Similarly, CNR values tended to be higher in the 2D TSE images, though not significantly (Figure 3b), and CV values were largely similar (Figure 3c).

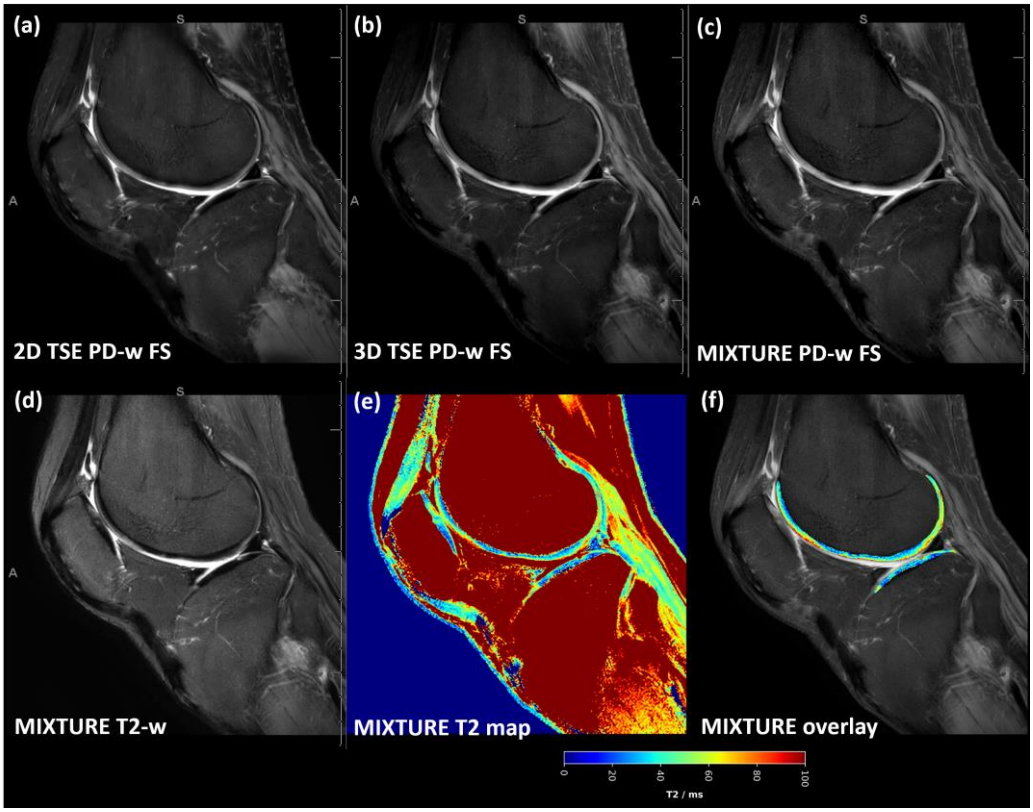

Figure 2. For a representative slice (through the central lateral femorotibial compartment) and joint, the 2D TSE image (**a**), the 3D TSE image (**b**), and the MIXTURE image (**c**) are shown alongside the MIXTURE T2-weighted image (**d**), the MIXTURE T2 map (**e**), and the segmented cartilage tissue overlay (**f**). In this example, the segmented femoral and tibial cartilage exhibited T2 relaxation times of 48 ± 18 ms and 36 ± 16 ms, respectively (mean ± standard deviation). In areas of fatty tissue, the MIXTURE T2 map did not yield meaningful values because SPAIR fat saturation was employed during the acquisition of the PD-weighted FS morphologic images. Abbreviations: PD—proton density, -w—weighted, FS—fat-saturated, MIXTURE—Multi-Interleaved X-prepared Turbo Spin-Echo with IntUitive Relaxometry, SPAIR—Spectral Attenuated Inversion Recovery. Figure S1 provides a close-up of the femoral and tibial cartilage of the weight-bearing region.

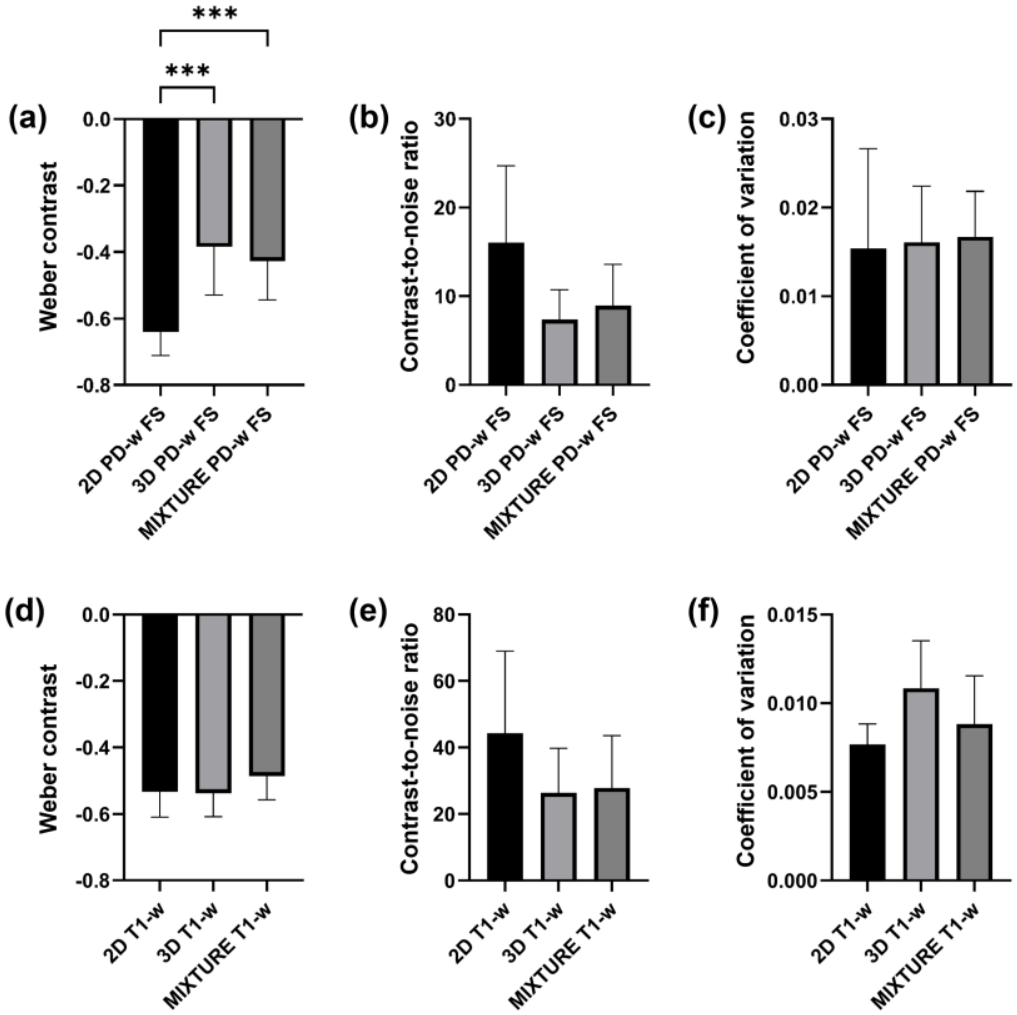

Figure 3. ROI-based comparisons were performed for the proton density-weighted (PD-w) fat-saturated (FS) sequences (**a**–**c**) and the T1-w sequences (**d**–**f**). (**a**,**d**) Weber contrast between cartilage and synovia (**a**) and cartilage and the infrapatellar fat pad (**d**). (**b**,**e**) Contrast-to-noise ratios between cartilage and synovia (**b**) and cartilage and the infrapatellar fat pad (**e**). (**c**,**f**) Coefficients of variation in synovial fluid (**c**) and the infrapatellar fat pad (**f**). Asterisks "***" indicate multiplicity-adjusted *p*-values $p \leq 0.001$. Bars and whiskers indicate means and standard deviations.

3.3. MIXTURE T1-Weighted Images Showed Slightly Increased Blurring

Across the acquired sequences, contrast, signal, and microstructural details appeared largely similar, although slightly more blurring was observed for the MIXTURE T1-w images (Figure 4 and Figure S2). Consequently, Weber contrast, CNR, and CV values were not significantly different (Figure 3d–f).

3.4. Quantitative Maps Showed Cartilage-Specific Zonal Stratification

Quantitative T2 maps of the femoral and tibial cartilage indicated a zonal stratification of the T2 relaxation times with decreasing values along increasing tissue depth (Figure S1e,f). Quantitative T1ρ maps of the cartilage indicated a depth-related zonal stratification, too (Figure S2e,f). Of note, the MIXTURE quantitative maps covered the whole joint.

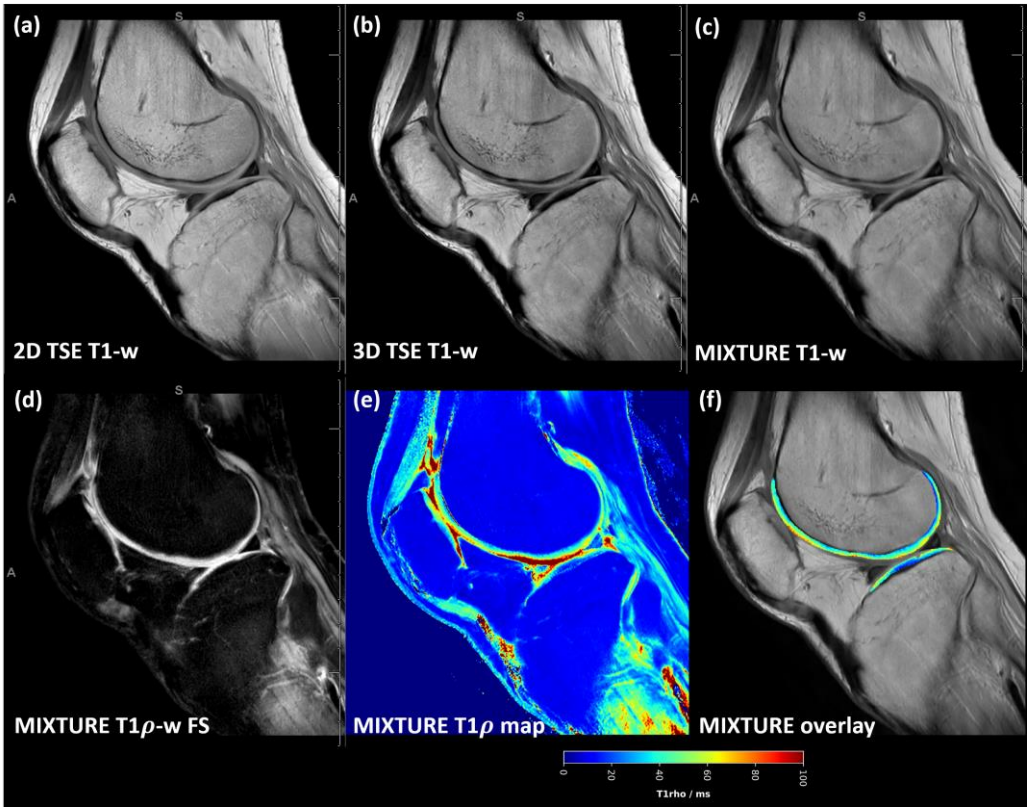

Figure 4. T1-weighted images acquired using the MIXTURE and corresponding reference sequences. The 2D TSE image (**a**), the 3D TSE image (**b**), and the MIXTURE image (**c**) are shown alongside the MIXTURE T1ρ-weighted fat-saturated image with 50 ms spin lock time (**d**), the MIXTURE T1ρ map (**e**), and the segmented cartilage tissue overlay (**f**). In this example, the segmented area of femoral and tibial cartilage exhibited mean T1ρ relaxation times of 45 ± 14 ms and 38 ± 14 ms, respectively (mean ± standard deviation). As for the MIXTURE T2 maps (Figure 2 and Figure S1), the MIXTURE T1ρ map did not yield meaningful values in areas of fatty tissue. Same slice and joint as in Figure 2. Abbreviations: -w—weighted, FS—fat saturated. MIXTURE—Multi-Interleaved X-prepared Turbo Spin-Echo with IntUitive Relaxometry. Supplementary Figure S2 provides a close-up of the femoral and tibial cartilage of the weight-bearing region.

3.5. Radiologists Assigned Equal or Higher Diagnostic Quality Scores to MIXTURE Sequences

3.5.1. PD-Weighted FS Images

Except for the collateral ligaments, the radiologists assigned evaluability scores of 4 or 5 on PD-w FS sequences, indicating "high" to "very high" evaluability with only slight inter-sequence differences (Table 2). Global diagnostic quality was largely rated as "very good" with median values of 5 [5; 5] (median [lower quartile; upper quartile]) for MIXTURE and 2D TSE PD-w FS vs. 5 [4; 5] for 3D TSE PD-w FS. One radiologist felt the additional T2 maps increased their diagnostic confidence in seven of ten assessed knee joints, while the other two radiologists considered them valuable in one and zero knee joints only, respectively. For the diagnostic evaluability scores, the highest EMM values, indicating overall higher scores, were found for the MIXTURE sequence (5.4 ± 0.8 [EMM ± standard error]), compared to the corresponding 2D TSE (5.1 ± 0.8) and 3D TSE (4.7 ± 0.8) sequences. Pair-wise post hoc tests indicated significantly higher diagnostic evaluability scores for MIXTURE than 3D TSE ($p < 0.001$). In contrast, no significant differences were found between 2D TSE and MIXTURE ($p = 0.055$) and 2D TSE and 3D TSE ($p = 0.019$). Evaluation of the global diagnostic quality score yielded EMM values of 7 ± 3, 10 ± 3, and 4 ± 3 for the MIXTURE, 2D TSE, and 3D TSE sequences, respectively, which were not significantly different (Table 3).

Table 2. Radiologic evaluation of image quality as a function of MR sequence and anatomic structure. The diagnostic evaluability scores for individual anatomic structures and the global diagnostic quality score are indicated as a function of image contrast and sequence (organized column-wise). Data are presented as median [lower quartile; upper quartile] of the readings by three radiologists who assigned scores for each specimen (n = 10).

	Scores	PD-w FS			T1-w		
		MIXTURE	2D TSE	3D TSE	MIXTURE	2D TSE	3D TSE
Diagnostic evaluability scores	MM posterior horn	5 [5; 5]	5 [5; 5]	5 [5; 5]	3 [3; 3]	3 [2; 3]	3 [2.25; 3]
	MM body region	5 [5; 5]	5 [5; 5]	5 [4; 5]	3 [2.25; 3]	3 [2; 3]	3 [2; 3]
	MM anterior horn	5 [5; 5]	5 [5; 5]	5 [5; 5]	3 [3; 3]	3 [3; 3]	3 [3; 3]
	LM posterior horn	5 [5; 5]	5 [5; 5]	5 [5; 5]	3 [2; 3]	3 [2; 3]	3 [2; 3]
	LM body region	5 [5; 5]	5 [4; 5]	5 [4; 5]	3 [2; 3]	3 [2; 3]	3 [2; 3]
	LM anterior horn	5 [5; 5]	5 [5; 5]	5 [5; 5]	3 [2.25; 3]	3 [2; 3]	3 [2; 3]
	Anterior cruciate ligament	5 [4.25; 5]	5 [4; 5]	4 [4; 4]	3 [2; 3]	3 [2; 3]	3 [2; 3]
	Posterior cruciate ligament	5 [5; 5]	5 [4; 5]	4.5 [4; 4.5]	3 [3; 3]	3 [3; 3]	3 [3; 3]
	Medial collateral ligament	2 [1.25; 2]	2 [1.25; 2]	2 [1.25; 2]	1 [1; 1]	1 [1; 1]	1 [1; 1]
	Lateral collateral ligament	3 [2; 3]	3 [2; 3]	3 [2; 3]	2.5 [1; 2.5]	2.5 [1.25; 2.5]	3 [1.25; 3]
	Medial femoral cartilage	5 [5; 5]	5 [5; 5]	5 [5; 5]	3 [3; 3]	3 [3; 3]	3 [3; 3]
	Lateral femoral cartilage	5 [5; 5]	5 [5; 5]	5 [5; 5]	3 [3; 3]	3 [3; 3]	3 [3; 3]
	Medial tibial cartilage	5 [5; 5]	5 [5; 5]	5 [5; 5]	3 [3; 3]	3 [3; 3]	3 [3; 3]
	Lateral tibial cartilage	5 [5; 5]	5 [5; 5]	5 [5; 5]	3 [3; 3]	3 [3; 3]	3 [3; 3]
	Trochlear cartilage	5 [5; 5]	5 [5; 5]	5 [5; 5]	3 [3; 3]	3 [3; 3]	3 [3; 3]
	Retropatellar cartilage	5 [5; 5]	5 [5; 5]	5 [5; 5]	3 [3; 3]	3 [3; 3]	3 [3; 3]
	Extensor mechanism	5 [5; 5]	5 [5; 5]	5 [4.25; 5]	4 [3; 4]	3.5 [3; 3.5]	3.5 [3; 3.5]
	Femoral bone marrow	4.5 [4; 4.5]	4 [4; 4]	4 [4; 4]	5 [5; 5]	5 [4; 5]	5 [4; 5]
	Tibial bone marrow	4.5 [4; 4.5]	4 [4; 4]	4 [4; 4]	5 [5; 5]	5 [4; 5]	5 [4; 5]
	Patellar bone marrow	4.5 [4; 4.5]	4 [4; 4]	4 [4; 4]	5 [5; 5]	5 [4; 5]	5 [4; 5]
	Synovium	5 [4; 5]	5 [4; 5]	5 [4; 5]	3 [3; 3]	3 [2; 3]	3 [2; 3]
	Effusion	5 [5; 5]	5 [5; 5]	5 [5; 5]	4 [3.25; 4]	3 [3; 3]	3 [3; 3]
Global diagnostic quality score		5 [5; 5]	5 [5; 5]	5 [4; 5]	5 [4.25; 5]	5 [5; 5]	5 [4; 5]

Please refer to Table 1 for sequence details. Additional abbreviations: MM—medial meniscus, LM—lateral meniscus.

Table 3. Post hoc analysis of the diagnostic scores. Based on the Cumulative Link Mixed Models, the diagnostic evaluability and overall diagnostic quality scores were compared in a pair-wise manner. The Tukey method was employed to correct for multiple comparisons by adjusting the significance levels of the pair-wise comparisons. Significant differences against the alpha threshold of 0.01 are marked in bold type.

Image Weighting	Score	2D TSE vs. 3D TSE	2D TSE vs. MIXTURE	3D TSE vs. MIXTURE
PD-w FS images	Diagnostic evaluability (per structure)	p = 0.019	p = 0.055	$\mathbf{p < 0.001}$
	Global diagnostic quality	p = 0.010	p = 0.294	p = 0.025
T1-w images	Diagnostic evaluability (per structure)	p = 0.999	$\mathbf{p < 0.001}$	$\mathbf{p < 0.001}$
	Global diagnostic quality	p = 0.056	p = 0.313	p = 0.565

3.5.2. T1-Weighted Images

The radiologists assigned an evaluability score of 5 to the bone marrow, while other structures mainly scored 3, indicating "intermediate evaluability", while the collateral ligaments were scored lower (Table 2). Nonetheless, the global diagnostic quality of all sequences was rated with a median score of 5, while only subtle differences were found for the lower quartiles. The radiologists' judgment on the potential of the MIXTURE T1ρ maps to increase diagnostic confidence was ambiguous as they reported additional diagnostic value in one, three, or nine assessed knee joints. The highest EMM values were found for the MIXTURE sequence (1.1 ± 0.6), which were significantly higher than those for the 2D TSE (0.3 ± 0.6) and 3D TSE (0.3 ± 0.6) sequences ($p < 0.001$). The EMM values of the 2D TSE and 3D TSE sequences did not differ significantly ($p = 0.999$). Evaluation of the global diagnostic quality score yielded EMM values of 2 ± 2, 3 ± 2, and 1 ± 2 for the MIXTURE, 2D TSE, and 3D TSE sequences, respectively, which did not differ significantly (Table 3).

3.6. Artificial Findings in Two Meniscal Posterior Horns

In two knee joint specimens, artificial findings of the meniscal posterior horns were noted for the MIXTURE and 3D TSE sequences, i.e., a fine hyperintense line extending from the meniscus base to the red–white zone that may principally be mistaken as a tear and a hyperintense area toward the meniscal undersurface that could be mistaken as degenerative meniscopathy. We consider these signal alterations artificial because they were absent in the corresponding 2D TSE and MIXTURE T2-weighted sequences (Figure 5). Yet, correlates were visible on the respective T1-w images.

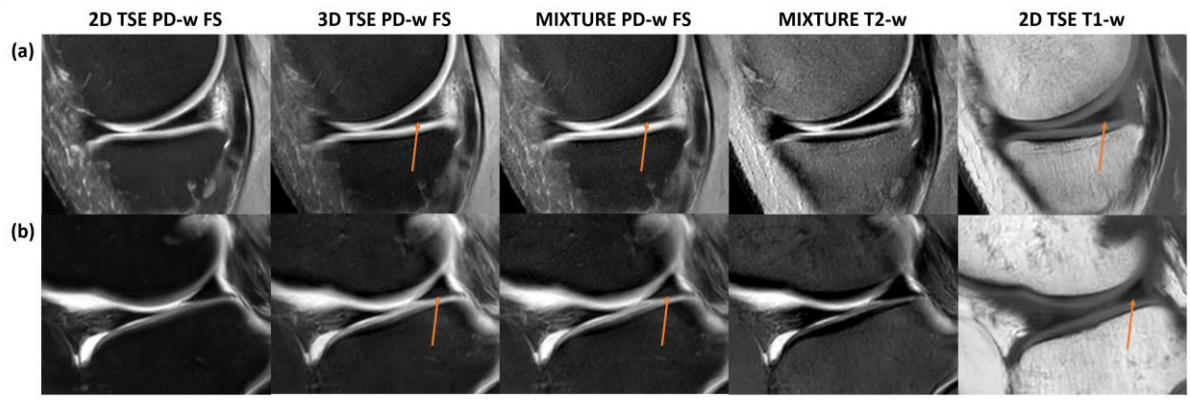

Figure 5. Artificial findings in the meniscal posterior horn. Fine linear structures of high signal intensity and variable size in the posterior horns of the medial (**a**) and lateral (**b**) meniscus (orange arrows) were only appreciable on the 3D TSE and MIXTURE PD-w FS images but not on the corresponding 2D TSE or MIXTURE T2-w images. These findings are likely artificial because of the missing correlate on the T2-w image. The hyperintense structural correlate on the T1-w images suggests that the 3D TSE and MIXTURE PD-w FS images depict residual T1 contrast, which can be due to the shorter relaxation times and the utilization of complex refocusing patterns compared to the 2D TSE PD-w FS sequence. The latter had a longer TR, increasing the likelihood of complete T1 relaxation.

4. Discussion

This study developed and refined two MIXTURE sequence variants combining PD-w FS or T1-w morphologic images with T2 mapping or T1ρ mapping, respectively. The variants matched our institution's knee protocol regarding image weightings and provided T2 and T1ρ maps of the whole joint in clinically feasible scan times. The most important finding of our study is that MIXTURE sequences were assigned similar or even significantly higher diagnostic evaluability and quality scores—both globally and per structure.

The MIXTURE platform is versatile because different image weightings can be included by selecting from different preparation modules. Other weightings beyond the

ones chosen in this study are feasible to reflect different practices. Previously, Sakai et al. combined PD-w images without fat saturation with T2-w FS images and T2 maps [15]. However, a MIXTURE sequence with FS yields meaningful T2 or T1ρ relaxation times only in non-fatty structures. Intentionally, we built non-isotropic MIXTURE variants, allowing for voxel-wise comparisons between the 2D and 3D sequences. Likewise, we aimed to show that MIXTURE sequences can compete with 2D TSE sequences from our institute's standard knee protocol while providing additional quantitative parameter maps. In that way, our study's design and direction differed from previously published MIXTURE studies [14–16]. However, while scientifically well-justified, this approach also meant we could not perform slice reconstruction in arbitrary orientations.

The proposed MIXTURE, 2D TSE, and 3D TSE sequences were similar in contrast-to-noise ratio, contrast, and coefficient of variation. While remaining contrast differences are likely not diagnostically detrimental because signal intensities can be manually adjusted, they result most from different sequence parameters. For example, the MIXTURE PD-w FS sequence used a shorter TR than the 2D TSE sequence to minimize the scan time yet was combined with a specific refocusing pattern to realize the familiar image appearance.

In contrast to previous studies investigating MIXTURE sequences in joint imaging, we used human cadaveric knee joint specimens for our evaluation. Compared to actual patient measurements, this approach limits the clinical translation of our findings. However, we found this model optimal for inter-sequence comparisons as the potential inter-sequence motion was effectively excluded, thereby improving standardization and comparability. Our radiologists noticed that the T2-weighted MIXTURE images looked "unnaturally" dark. This finding is plausible as human tissues, when imaged at room temperature, have substantially reduced contrast between fat and muscle (on T2-w images), while the contrast between fat and fluid increases [22]. When acquired in a healthy volunteer, the images demonstrated familiar characteristics and contrasts.

Semi-quantitatively, we found similar (per-structure) evaluability and (global) diagnostic quality scores between the sequences. To the best of our knowledge, this study is the first to include a comparative reader study between MIXTURE sequences and clinical reference sequences, thereby expanding the evidence supporting the diagnostic quality of MIXTURE. However, qualitatively, the readers' opinions on the utility of the quantitative parameter maps were ambiguous. While one radiologist considered them largely beneficial, the other two reported the opposite, which may reflect that (i) clinical diagnosis still relies exclusively on morphologic sequences and (ii) new sequences need familiarization (beyond mere clinical adoption) to be considered beneficial. To fit into clinical workflows, the quantitative parameter maps must be amenable to automated segmentation approaches, which could be facilitated by isotropic morphologic MIXTURE images. Computer-aided and deep-learning enhanced segmentation models may be available in the near future [23,24].

In the MIXTURE and 3D TSE PD-w FS sequences, we observed hyperintense intrameniscal signal alterations in two knee joints. These signal alterations were absent in the 2D TSE sequence, indicating their artificiality. While MIXTURE T2-w images confirmed these as artificial, their cause remains uncertain. We speculate that residual T1 contrast may have produced these artifacts, evidenced by hyperintense correlates on the T1-w images and possibly amplified by the 3D sequence refocusing patterns and shorter TRs (of the MIXTURE and 3D TSE). Future research should explore the nature of these artifacts, e.g., by using longer TR or different refocusing patterns. Importantly, MIXTURE T2-weighted and PD-weighted FS images are already available from the same sequence. This circumstance favors the clinical use of MIXTURE sequences, as our current standard protocols without MIXTURE sequences require the additional acquisition of T2-weighted sequences to determine the nature and artificiality of intrameniscal signal alterations.

In addition to cartilage imaging and osteoarthritis, combined sequences such as MIXTURE hold promise for assessing other musculoskeletal conditions. When integrated into combined sequences, quantitative parameter maps, particularly T2 and T1rho maps, offer valuable insights into tissue composition, integrity, and physiological changes. Beyond

cartilage, these capabilities make MIXTURE particularly interesting for conditions characterized by alterations in tissue microstructure, such as inflammatory arthritis, ligament and tendon injuries, and meniscal tears [25], and for muscle assessment (e.g., neuromuscular diseases) [26,27]. Beyond the musculoskeletal system, these capabilities may be interesting for neuroimaging (e.g., multiple sclerosis and other neurodegenerative conditions) [28], cardiovascular imaging (e.g., myocardial tissue viability and function) [29], and oncology imaging (e.g., early detection and characterization of tumors) [30].

Our study has limitations. First, the specimen size and type were limited as cadavers are not fully representative of the conditions in patients. Similarly, pathological variability was limited, and consequently, we consider this study a proof-of-concept that needs to be followed by future patient studies. Second, the design of our reader study ignored that some structures within the knee joint are routinely judged based on PD-w FS or T1-w sequences only. Radiologists were instructed to subjectively assess a given structure and assign lower scores if a structure was poorly evaluable. Most intra-articular structures, such as the menisci and cartilage, are routinely evaluated on the PD-w FS sequences, which explains their higher scores. Third, we only evaluated one clinical 3T MRI scanner and coil. The sequence's usability for different MRI scanners, field strengths, and coils remains to be studied. Fourth, we could not validate MIXTURE's T2 and T1ρ relaxation times against nominal relaxation times obtained by reference sequences. Ideally, a phantom with known relaxation times [31] and appropriate geometry (to fit into the knee coil) would be used to study the validity of the quantitative approaches versus reference sequences such as multi-echo-spin-echo T2 mapping sequences and alternative combined sequences such as qDESS. Yet, most commercially available phantoms are head-sized. Also, there is no consensus about T1ρ reference sequences yet, because of multiple technical confounders that may affect both MIXTURE and reference sequences [32]. Fifth, this study could not evaluate the susceptibility of MIXTURE sequences to blood flow and motion because of the study's in situ nature. The sixth limitation involves the choice of specific echo and spin lock times, which were not optimized for maximized acquisition efficiency. Our MIXTURE sequence combining T1-weighted imaging with T1rho mapping used three spin lock times and required a longer imaging time than the one combining PD-weighted imaging with T2 mapping, which used two echo times only. This choice was based on the available literature [14–16]. There is a trade-off between the number of echoes or spin lock times, respectively, and the accuracy of the quantitative parameter maps, which has to be investigated in future studies.

5. Conclusions

In conclusion, the MIXTURE sequence platform provides (i) morphologic images of diagnostic quality and adjustable TSE-based contrasts to be aligned with a radiologist's or institution's practices and (ii) quantitative parameter mapping with whole-joint coverage and additional insights on soft tissue composition and ultrastructure in clinically feasible scan times. By increasing diagnostic efficiency, MIXTURE provides a versatile approach to include quantitative MRI techniques in clinical routine protocols.

Supplementary Materials: The following supporting information can be downloaded at: https://www.mdpi.com/article/10.3390/diagnostics14100978/s1, Figure S1: Close-up of the central weight-bearing region (proton density-weighted fat-saturated MIXTURE and corresponding reference sequences); Figure S2: Close-up of the central weight-bearing joint region (T1-weighted MIXTURE and reference sequences).

Author Contributions: Conceptualization S.N. and T.L.; Methodology T.L., S.Z., M.Y. and S.N.; Software T.L., M.Y. and S.Z.; Validation D.T. and S.N.; Formal Analysis N.P., K.L.R., T.L. and S.N.; Investigation N.P., M.H., M.P. and C.Y.; Resources C.K. and A.P.; Data Curation N.P.; Writing (Original Draft) T.L.; Writing (Review and Editing) T.L., N.P., S.N., R.S. and S.N.; Visualization N.P. and T.L.; Supervision S.N., D.T., C.K. and A.P.; Project Administration T.L. and S.N.; Funding Acquisition T.L., S.N. and D.T. All authors have read and agreed to the published version of the manuscript.

Funding: This work was supported by the START program of the Faculty of Medicine of the RWTH Aachen University (No. 692316). DT is supported by the European Union's Horizon Europe programme (ODELIA, 101057091), by grants from the Deutsche Forschungsgemeinschaft (DFG) (TR 1700/7-1), and the German Federal Ministry of Education and Research (SWAG, 01KD2215A; TRANSFORM LIVER, 031L0312A). SN is funded by grants from the Deutsche Forschungsgemeinschaft (DFG) (NE 2136/3-1).

Institutional Review Board Statement: The study was conducted in accordance with the Declaration of Helsinki, and approved by the Ethics Committee, RWTH Aachen University, EK180/16.

Informed Consent Statement: Body donors gave written informed consent prior to the initiation of the study.

Data Availability Statement: The datasets used and/or analyzed during the current study are available from the corresponding author (T.L.) upon reasonable request.

Acknowledgments: The authors would like to acknowledge the support of David Haas and Sarah Nüsser from the Institute of Molecular and Cellular Anatomy, RWTH Aachen University.

Conflicts of Interest: Shuo Zhang and Masami Yoneyama are employees of Philips. The remaining authors declare that the research was conducted in the absence of any commercial or financial relationships that could be construed as a potential conflict of interest.

References

1. March, L.; Cross, M.; Lo, C.; Arden, N.K.; Gates, L.; Leyland, K.M.; Hawker, G.; King, L.; Leyland, K. OARSI Osteoarthritis Research Society International. Osteoarthritis: A Serious Disease, Submitted to the U.S. Food and Drug Administration 1 December 2016. Available online: https://www.oarsi.org/sites/default/files/docs/2016/oarsi_white_paper_oa_serious_disease_121416_1.pdf (accessed on 2 May 2024).
2. Braun, H.J.; Gold, G.E. Diagnosis of osteoarthritis: Imaging. *Bone* **2012**, *51*, 278–288. [CrossRef] [PubMed]
3. Wenham, C.Y.J.; Grainger, A.J.; Conaghan, P.G. The role of imaging modalities in the diagnosis, differential diagnosis and clinical assessment of peripheral joint osteoarthritis. *Osteoarthr. Cartil.* **2014**, *22*, 1692–1702. [CrossRef]
4. Guermazi, A.; Alizai, H.; Crema, M.; Trattnig, S.; Regatte, R.; Roemer, F. Compositional MRI techniques for evaluation of cartilage degeneration in osteoarthritis. *Osteoarthr. Cartil.* **2015**, *23*, 1639–1653. [CrossRef] [PubMed]
5. Binks, D.; Hodgson, R.; Ries, M.; Foster, R.; Smye, S.; McGonagle, D.; Radjenovic, A. Quantitative parametric MRI of articular cartilage: A review of progress and open challenges. *Br. J. Radiol.* **2013**, *86*, 20120163. [CrossRef] [PubMed]
6. Thüring, J.; Linka, K.; Itskov, M.; Knobe, M.; Hitpaß, L.; Kuhl, C.; Truhn, D.; Nebelung, S. Multiparametric MRI and Computational Modelling in the Assessment of Human Articular Cartilage Properties: A Comprehensive Approach. *BioMed Res. Int.* **2018**, 9460456. [CrossRef] [PubMed]
7. Le, J.; Peng, Q.; Sperling, K. Biochemical magnetic resonance imaging of knee articular cartilage: T1rho and T2 mapping as cartilage degeneration biomarkers. *Ann. N. Y. Acad. Sci.* **2016**, *1383*, 34–42. [CrossRef] [PubMed]
8. Hager, B.; Raudner, M.; Juras, V.; Zaric, O.; Szomolanyi, P.; Schreiner, M.; Trattnig, S. MRI of Early OA. In *Early Osteoarthritis: State-of-the-Art Approaches to Diagnosis, Treatment and Controversies*; Springer: Cham, Switzerland, 2022; pp. 17–26.
9. Kijowski, R.; Blankenbaker, D.G.; Rio, d.M.A.; Baer, G.S.; Graf, B.K. Evaluation of the Articular Cartilage of the Knee Joint: Value of Adding a T2 Mapping Sequence to a Routine MR Imaging Protocol. *Radiology* **2013**, *267*, 503–513. [CrossRef] [PubMed]
10. Alsayyad, M.A.I.; Shehata, K.A.A.; Khattab, R.T. Role of adding T2 mapping sequence to the routine MR imaging protocol in the assessment of articular knee cartilage in osteoarthritis. *Egypt. J. Radiol. Nuclear Med.* **2021**, *52*, 78. [CrossRef]
11. Nevitt, M.C.; Felson, D.T.; Lester, G. The Osteoarthritis Initiative: Protocol for the Cohort Study. Available online: https://nda.nih.gov/static/docs/StudyDesignProtocolAndAppendices.pdf (accessed on 2 September 2022).
12. Chaudhari, A.; Stevens, K.; Sveinsson, B.; Wood, J.; Beaulieu, C.; Oei, E.; Rosenberg, J.; Kogan, F.; Alley, M.; Gold, G.; et al. Combined 5-minute double-echo in steady-state with separated echoes and 2-minute proton-density-weighted 2D FSE sequence for comprehensive whole-joint knee MRI assessment. *J. Magn. Resonance Imaging* **2019**, *49*, 183–194. [CrossRef]
13. Chaudhari, A.S.; Grissom, M.J.; Fang, Z.; Sveinsson, B.; Lee, J.H.; Gold, G.E.; Hargreaves, B.A.; Stevens, K.J. Diagnostic Accuracy of Quantitative Multicontrast 5-Minute Knee MRI Using Prospective Artificial Intelligence Image Quality Enhancement. *Am. J. Roentgenol.* **2021**, *216*, 1614–1625. [CrossRef]
14. Yoneyama, M.; Sakai, T.; Zhang, S.; Murayama, D.; Yokota, H.; Zhao, Y.; Saruya, S.; Suzuki, M.; Watanabe, A.; Niitsu, M.; et al. MIXTURE: A novel sequence for simultaneous morphological and quantitative imaging based on multi-interleaved 3D turbo-spin echo MRI. *Proc. ISMRM* **2021**, *2021*, 4203.
15. Sakai, T.; Yoneyama, M.; Watanabe, A.; Murayama, D.; Ochi, S.; Zhang, S.; Miyati, T. Simultaneous anatomical, pathological and T2 quantitative knee imaging with 3D submillimeter isotropic resolution using MIXTURE. *Proc. ISMRM* **2021**, *2021*, 0845.
16. Saruya, S.; Suzuki, M.; Yoneyama, M.; Inoue, K.; Kozawa, E.; Niitsu, M. 3D sub-millimeter isotropic knee cartilage T1rho mapping using multi-interleaved fluid-attenuated TSE acquisition (MIXTURE). *Proc. ISMRM* **2021**, *2021*, 2977.

17. Gupta, S.; Porwal, R. Appropriate Contrast Enhancement Measures for Brain and Breast Cancer Images. *Int. J. Biomed. Imaging* **2016**, *2016*, 4710842. [CrossRef] [PubMed]
18. Weiss, J.; Notohamiprodjo, M.; Martirosian, P.; Taron, J.; Nickel, M.D.; Kolb, M.; Bamberg, F.; Nikolaou, K.; Othman, A.E. Self-Gated 4D-MRI of the Liver: Initial Clinical Results of Continuous Multiphase Imaging of Hepatic Enhancement. *J. Magn. Resonance Imaging* **2018**, *47*, 459–467. [CrossRef] [PubMed]
19. Yushkevich, P.A.; Piven, J.; Hazlett, H.C.; Smith, R.G.; Ho, S.; Gee, J.C.; Gerig, G. User-guided 3D active contour segmentation of anatomical structures: Significantly improved efficiency and reliability. *NeuroImage* **2006**, *31*, 1116–1128. [CrossRef] [PubMed]
20. Available online: http://cran.nexr.com/web/packages/emmeans/vignettes/basics.html (accessed on 27 September 2023).
21. Available online: https://cran.r-project.org/web/packages/emmeans/vignettes/sophisticated.html#ordinal (accessed on 27 September 2023).
22. Ruder, T.; Thali, M.; Hatch, G. Essentials of forensic post-mortem MR imaging in adults. *Br. J. Radiol.* **2014**, *87*, 20130567. [CrossRef]
23. Schock, J.; Kopaczka, M.; Agthe, B.; Huang, J.; Kruse, P.; Truhn, D.; Conrad, S.; Antoch, G.; Kuhl, C.; Nebelung, S.; et al. A Method for Semantic Knee Bone and Cartilage Segmentation with Deep 3D Shape Fitting Using Data from the Osteoarthritis Initiative. In *Shape in Medical Imaging. ShapeMI 2020. Lecture Notes in Computer Science*; Reuter, M., Wachinger, C., Lombaert, H., Paniagua, B., Goksel, O., Rekik, I., Eds.; Springer: Cham, Switzerland, 2020.
24. Desai, A.D.; Barbieri, M.; Mazzoli, V.; Rubin, E.; Black, M.S.; Watkins, L.E.; Gold, G.E.; Hargreaves, B.A.; Chaudhari, A.S. DOSMA: A deep-learning, open-source framework for musculoskeletal MRI analysis. In Proceedings of the 27th Annual Meeting ISMRM, Montreal, QC, Canada, 10–13 May 2019.
25. Barendregt, A.M.; Bray, T.J.P.; Hall-Craggs, M.A.; Maas, M. Emerging quantitative MR imaging biomarkers in inflammatory arthritides. *Eur. J. Radiol.* **2019**, *121*, 108707. [CrossRef]
26. de Mello, R.; Ma, Y.; Ji, Y.; Du, J.; Chang, E.Y. Quantitative MRI Musculoskeletal Techniques: An Update. *AJR* **2019**, *213*, 524–533. [CrossRef]
27. Schlaeger, S.; Weidlich, D.; Klupp, E.; Montagnese, F.; Deschauer, M.; Schoser, B.; Bublitz, S.; Ruschke, S.; Zimmer, C.; Rummeny, E.J.; et al. Water T2 Mapping in Fatty Infiltrated Thigh Muscles of Patients With Neuromuscular Diseases Using a T2-Prepared 3D Turbo Spin Echo With SPAIR. *J. Magn. Resonance Imaging* **2020**, *51*, 1727–1736. [CrossRef]
28. Seiler, A.; Nöth, U.; Hok, P.; Reiländer, A.; Maiworm, M.; Baudrexel, S.; Meuth, S.; Rosenow, F.; Steinmetz, H.; Wagner, M.; et al. Multiparametric Quantitative MRI in Neurological Diseases. *Front. Neurol.* **2021**, *12*, 640239. [CrossRef] [PubMed]
29. Ogier, A.C.; Bustin, A.; Cochet, H.; Schwitter, J.; van Heeswijk, R.B. The Road Toward Reproducibility of Parametric Mapping of the Heart: A Technical Review. *Front. Cardiovasc. Med.* **2022**, *9*, 876475. [CrossRef] [PubMed]
30. Yankeelov, T.E.; Pickens, D.R.; Price, R.R. (Eds.) *Quantitative MRI in Cancer*; CRC Press Inc.: Boca Raton, FL, USA, 2011.
31. Obuchowski, N.A.; Reeves, A.P.; Huang, E.P.; Wang, X.-F.; Buckler, A.J.; Kim, H.J.; Barnhart, H.X.; Jackson, E.F.; Giger, M.L.; Pennello, G.; et al. Quantitative imaging biomarkers: A review of statistical methods for computer algorithm comparisons. *Stat. Methods Med. Res.* **2015**, *24*, 68–106. [CrossRef] [PubMed]
32. Chen, W. Errors in quantitative T1rho imaging and the correction methods. *Quant. Imaging Med. Surg.* **2015**, *5*, 583–591. [PubMed]